Plasmonics in Sensing: From Colorimetry to SERS Analytics

Christian Kuttner

Abstract

This chapter gives a brief overview of plasmonic nanoparticle (NP)-based sensing concepts ranging from classical spectral-shift colorimetry to the highly active field of surface-enhanced Raman scattering (SERS) spectroscopy. In the last two decades, particularly colloidal approaches have been developed, for example for refractive-index sensing, detection of ad–/desorption and ligand-exchange processes, as well as ultrasensitive chemical sensing utilizing well-defined nanocrystals or discrete self-assembled superstructures in 2D and 3D. Apart from individual NPs, the rational design of self-assembled nanostructures grants spectroscopic access to unprecedented physicochemical information. This involves selected research examples on molecular trapping, ligand corona analysis, SERS-encoding, and biosensing. The origin of the SERS effect, also in regard of hot spots formation by off-resonant excitation, is reviewed and discussed in the context of the current challenge to formulate a generalized metric for high SERS efficiency. Special emphasis lies on addressing the fundamental design criteria and the specific challenges of these particle-based sensing techniques.

Keywords: colorimetry, SERS, LSPR, colloidal sensors, optically functional materials, self-assembled nanostructures

1. Introduction

The field of plasmonics has advanced immensely over the years and is spreading more and more into the area of sensor technology [1–4]. This is due to the unique interaction of light with noble metals [5]. The excitation of conduction electrons to perform collective vibrations, both in volume as well as at the surface, shows in brilliant colors, which have fascinated

people since the medieval times. Countless prominent examples of art objects still exist today, for example the Lycurgus Cup (4th century AD) or stained-glass windows of cathedrals.

As early as 1857, Michael Faraday published his groundbreaking findings (The Bakerian Lecture of the Royal Society of London [6]) on the experimental interactions of gold and other metals with light [7]. "*Light has a relation to the matter which it meets with in its course, and is affected by it, being reflected, deflected, transmitted, refracted, absorbed, etc. by particles very minute in their dimensions* [6]." He studied the emergence of different colors for *fluids containing gold reduced to diffused particles* and described the *metallic character of the divided gold*: "*Hitherto it may seem that I have assumed the various preparations of gold, whether ruby, green, violet, or blue in color, to consist of that substance in a metallic divided state* [6]."

Between 1900 and 1920, the famous contributions of James Clerk Maxwell-Garnett [8], Gustav Mie [9], Richard Gans [10, 11], and Richard Adolf Zsigmondy [12], just to name a few, proved that plasmonic colors were based on optical resonances that occur for particles smaller than the wavelength of light and that can be theoretically described and precisely predicted [13–15]. This gave birth to the field of colloidal plasmonic nanoscience [16]. Over the last decades, a variety of different nanostructures, both in the form of individual NPs and particle assemblies [17], have been developed with a special focus on their use as colorimetric or SERS spectroscopy sensors [18, 19].

Today's pronounced diversity of available nanostructures demonstrates the high level of interest in these *optically functional materials*. Within the scope of this book chapter, this diversity can, of course, only be covered to a limited extent. For this reason, the focus here is on NPs as defined building blocks for discrete nanostructures by guided self-assembly [20–22]. **Figure 1** provides a rough overview of functional structures which have been found to be particularly suitable for sensor applications. The first area is represented by individual nanocrystals, for example in spherical, rod-shaped, triangular, or star-shaped morphologies with strong *intrinsic* electromagnetic hot spots. This can be extended by coupling these particles to a metal surface or thin-film, the formation of branched structures by overgrowth, or hollow, core/shell, and nested structures with nanoscale interior gaps. Nanoparticles at short distances form *extrinsic* hot spots by strong electromagnetic interactions [23], referred to as plasmonic coupling [24]. Even in the disordered state, particle aggregates produce strong field enhancements. However, it is the ordered assembly of particles that allows plasmonic hybridization to emerge [25]. Hybridization can result in highly sensitive modes for spectral shift sensing and intense near-field enhancement for chemical sensing [14]. Again, the diversity ranges from discrete single nanoclusters with uniform coordination numbers to complex superstructures, supercrystals, and patterned structures both in 2D and 3D, which can be fabricated by colloidal engineering.

In this chapter, we will first address the field of plasmonic colorimetric sensing. Here, the fundamental concepts for sensing of surface plasmon resonances of metallic thin films are reviewed and then extended to localized surface plasmon resonances [26] of NPs and ordered NP assemblies by guided self-assembly [20–22]. Second, we review SERS analytics divided into several steps: the first principles of SERS [27] and off-resonance excitation, SERS analytics of dispersed particles with a focus of the tasks of functional shells, SERS analytics using disordered aggregates under controlled conditions, and finally ordered assemblies designed for high SERS activity [28, 29].
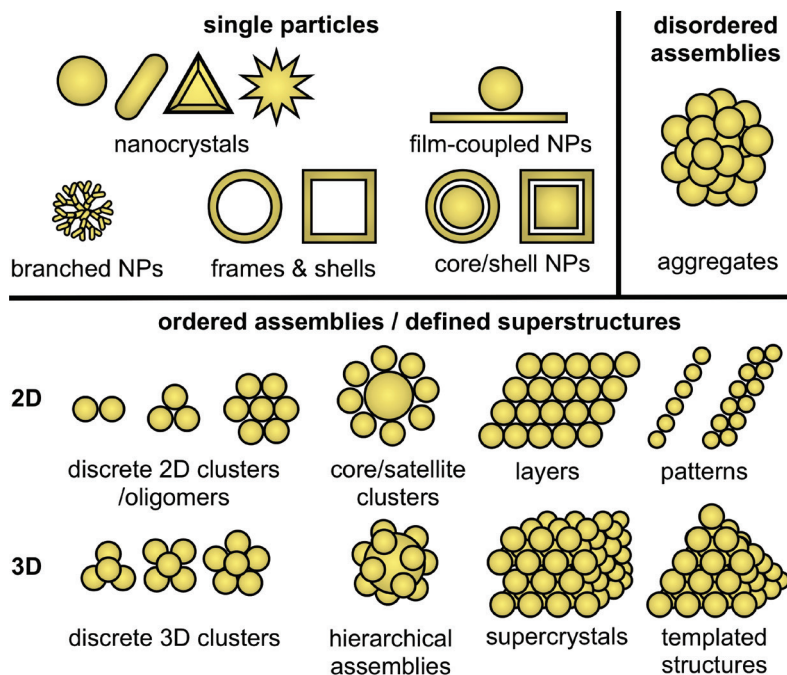
Figure 1. Schematic overview of the diversity in plasmonic nanoparticles and -structures: (top, left) nanocrystals, film-coupled particles, and hollow/nested morphologies on single particle level; (top, right) disordered assemblies of aggregated NPs; (bottom) ordered assemblies of discrete NP oligomers, clusters, and defined superstructures in 2D and 3D.

2. Plasmonic colorimetric sensing

To begin with, we will first briefly review SPR spectroscopy of thin metallic films as a foundation for LSPR spectroscopy. Colorimetric sensing describes the optical determination of chemical or physicochemical properties of a sample. Subsequently, we will discuss concepts in which the plasmonic response is used to obtain information at interfaces or at the near-field environment of metal structures, which would otherwise be inaccessible.

2.1. SPR spectroscopy of thin metal films

Surface plasmons (SPs) are electromagnetic waves, emerging from surface plasmon resonances (SPRs), that propagate along the surface or interface of a conductor, usually a metal/dielectric interface [30]. Essentially, surface plasmons are light waves *trapped at interfaces* because of their strong interaction with the free electrons of the conductor. Surface structuring can guide this interaction [31]. The response of the free electrons takes place collectively in form of oscillations in resonance with the light wave. The consequent charge density oscillation at the surface leads to a concentration of light and thus an enhancement of the local electric nearfield. The high sensitivity of this light-matter interaction renders it attractive for sensing applications. SP-based sensing builds on a *simple* resonance condition:

$$k_{\mathrm{sp}} = k_0 \cdot \sqrt{\frac{\varepsilon_{\mathrm{d}}\ \varepsilon_{\mathrm{m}}}{\varepsilon_{\mathrm{d}} + \varepsilon_{\mathrm{m}}}}$$

(1)

The resonance condition requires the SP mode (with frequency-dependent wave-vector k_{sp}) to be greater than that of a free-space photon of the same frequency (free-space wave-vector k_0). In addition, for SPRs, the frequency-dependent permittivity of metal (ε_{m}) and dielectric (ε_{d}) need to be of opposite signs. As a consequence, the SP resonance phenomenon has been employed for biochemical sensing [32] and clinical diagnosis [33]. Under appropriate conditions, the reflectivity of a thin metal film is extremely sensitive to changes in the local refractive index environment. **Figure 2A** (left) shows an exemplary SPR sensor in a fluidic channel in Kretschmann configuration, using a prism for coupling p-polarized light into the metallic film interface [34]. The resulting evanescently decaying field reaches beyond the metallic interface into the sensing medium. When the SPR condition is satisfied, the reflection spectrum for monochromic light shows a characteristic resonance dip (**Figure 2A**, right). Here, the resonance condition is
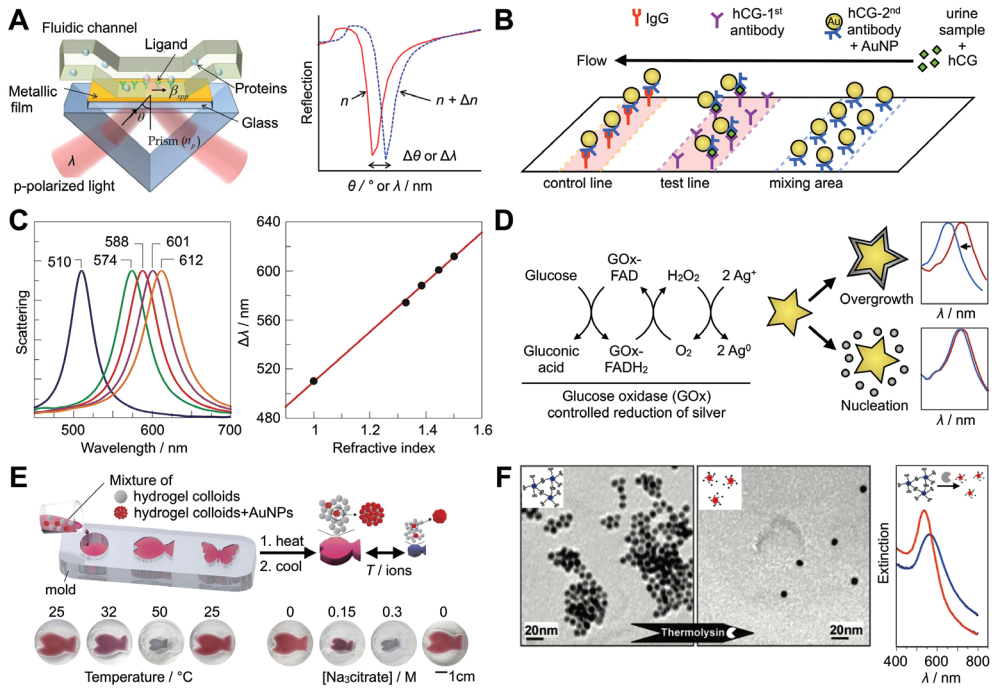

Figure 2. Fundamental concepts of colorimetric plasmonic sensing. (A) SPR sensor in a fluidic channel. Copyright 2011 MDPI, adapted with permission [34]. (B) Pregnancy test using AuNPs as inert dye. (C) Refractive index sensitivity of an AgNP-based optical sensor. Copyright 2003 ACS, adapted with permission [44]. (D) LSPR sensor concept for enzyme-guided inverse sensitivity [45]. (E) Dual-responsive hydrogel/AuNP hybrid particles. Copyright 2016 NPG, adapted with permission [47]. (F) Protease-triggered dispersion of AuNP assemblies. Copyright 2007 ACS, adapted with permission [48].

$$\frac{2\,\pi}{\lambda} \cdot n_{\mathrm{p}} \cdot \sin\theta = \mathrm{Re}\left(\frac{\omega}{\mathrm{c}} \cdot \sqrt{\frac{n_{\mathrm{s}}^2\,\varepsilon_{\mathrm{m}}}{n_{\mathrm{s}}^2 + \varepsilon_{\mathrm{m}}}}\right)$$

(2)

where n denotes the refractive indices of the dielectric prism (p) and the sensing medium (s), λ is the wavelength in free space, and θ is the incident angle of light [34]. Thus, changes of the refractive index (Δn) of the sensing medium will shift the resonance dip by altering the resonance angle ($\Delta\theta$) and/or the resonance wavelength ($\Delta\lambda$). The sensing of this resonant spectral response can be realized in different micro- and nanostructured sensor configurations (e.g., prism-, waveguide-, channel-, grating-based setups) [35]. Oates et al. demonstrated that the established methods of SPR spectroscopy for chemical and biological sensing can be enhanced by using the ellipsometric phase information [31]. Next, we focus on colorimetric sensing using plasmonic NPs.

2.2. LSPR spectroscopy of single NPs and disordered NP assemblies

The transition from SPR to localized surface plasmon resonance (LSPR) sensing is accompanied by the step from sensors using metallic thin-films to nanosensors in the form of particulate matter [36–38]. The plasmon generated on a small nanoparticle, for example, a sphere, experiences strong spatial confinement because of its hindered and limited propagation [39]. This confinement, also known as localization, results in discrete charge density oscillations [9, 40], which manifest themselves by intensive colors [41]. The excitation frequency of localized plasmons (absorbance band) is highly sensitive for the size, shape, composition, and refractive index environment of the NP. Though LSPRs were capitalized for various nanophotonic applications covering many fields [16, 26, 42], this chapter is limited to their use as sensor elements. For this purpose, we briefly survey the most commonly used and prominent concepts for colorimetric sensing.

Figure 2 summarizes the fundamental colorimetric sensing concepts using single NPs and disordered NP assemblies. The first example shows the working principle of a pregnancy test for which AuNPs (conjugated to anti-hCG antibodies, blue) serve as an inert dye to detect the presence of hCG antigens (**Figure 2B**) [43]. The test is basically a lateral flow sandwich immunoassay consisting of a test line with anti-hCG antibodies (violet), a control line with immunoglobulin G (IgG, red) antibodies, and a mixing with immobilized anti hCG-conjugated AuNPs. By application of a urine sample, the NPs bind to available hCG antigens (which are indicative for a pregnancy). This is followed by the selective binding of AuNPs to the control and test line, while the latter only happens in the presence of hCG antibodies. In this example, the AuNPs serve as an inert dye, which does not interfere with the antibody–antigen binding by biorecognition and possesses high chemical stability.

Figure 2C highlights the refractive index sensitivity of an AgNP-based optical sensor in various solvent environments (left) [44]. Van Duyne et al. found a linear relationship between the refractive index environment and the LSPR position. This enabled to detect the adsorption of fewer than 60.000 1-hexadecanethiol molecules on single AgNPs which corresponded to a 41 nm shift followed by dark-field spectroscopy. However, for ultralow concentrations, the variations in the physical property (e.g., LSPR shift) become increasingly smaller, and

thus, harder to detect with confidence. Contrary to conventional transducers which generate a signal that is directly proportional to the concentration of the target molecule, Stevens and coworkers proposed an LSPR sensor with inverse sensitivity (**Figure 2D**) [45]. The key for this inverse sensitivity is the enzymatic control over the rate of nucleation of Ag on Au nanostars (top: overgrowth; bottom: nucleation), accompanied by a blueshift of the LSPR. Different biosensing strategies have been proposed building on enzymatic reactions and NPs [46].

Apart from dispersed NPs, the plasmonic coupling between NPs, which is depending on their spatial interspacings, can be utilized for colorimetry. Song and Cho reported dual-responsive architectures by mixing hydrogel and AuNP-decorated hydrogel particles (**Figure 2E**) [47]. This hybrid ensemble responds to both temperature and ions by means of a volume and color change in aqueous systems. Both stimuli can be used to reversibly trigger the transition of uncoupled well-separated AuNPs (red tint) to a state that allows for plasmonic coupling (blue tint), mediated by the hydrogel matrix. Ulijn and Stevens et al. demonstrated the bioresponsive transition from aggregated to dispersed state [48]. **Figure 2F** shows the protease-triggered dispersion of AuNP assemblies using thermolysin for the removal of attractive self-assembly groups and revelation of repulsive charged groups. The consequent blueshift of the LSPR allowed for simple and highly sensitive detection of the presence of thermolysin, which could be tailored for different proteases.

Another approach builds on measuring the orientation of a sample. For this, it is necessary to align the ensemble of NPs macroscopically. This was achieved for anisotropic NPs homogenously dispersed in an elastic polymer matrix [49, 50]. By uniaxial stretching of the material, the NPs are oriented along the direction of elongation. As a result, the material exhibits uniform plasmonic response, which enables to optically detect the orientation of the material. In the following, we will continue with assemblies containing ordered NPs and patterns.

2.3. LSPR spectroscopy of ordered NP assemblies and defined patterned superstructures

Figure 3 highlights colorimetric sensing examples of ordered NP assemblies and defined patterned superstructures. Because the LSPR depends on the local dielectric environment at the NP surface, the LSPR shift can be evaluated to detect changes in effective refractive index. The first example is a macroscopic *plasmonic library* consisting of well-separated non-coupling AuNPs with a gradient in size, induced by Au overgrowth [51]. Along the array, the size increase goes along with a color change from colorless to pink (**Figure 3A**, left). Aided by electromagnetic simulations, it was possible to evaluate the effective refractive index and thus changes in the local density of the hydrogel shell around the substrate-supported particles (right). The initial increase of the refractive index indicated a densification of the hydrogel network upon particle growth from 10 to 30 nm. The subsequent decrease above 30 nm might result from internal breakup/rupture of the network.

Sönnichsen et al. proposed the use of core/satellite assemblies for highly sensitive refractive index sensing [52]. **Figure 3B** (left) shows 60 nm AuNPs as cores linked to 20 nm AuNPs as satellites. The average number of satellites allowed tuning the LSPR from 543 to 575 nm. The core/satellite nanostructures showed about twofold higher colorimetric sensitivity ($\Delta\lambda/\Delta n$) than similar sized gold NPs (right). Lee et al. developed a theory-based design of such core/
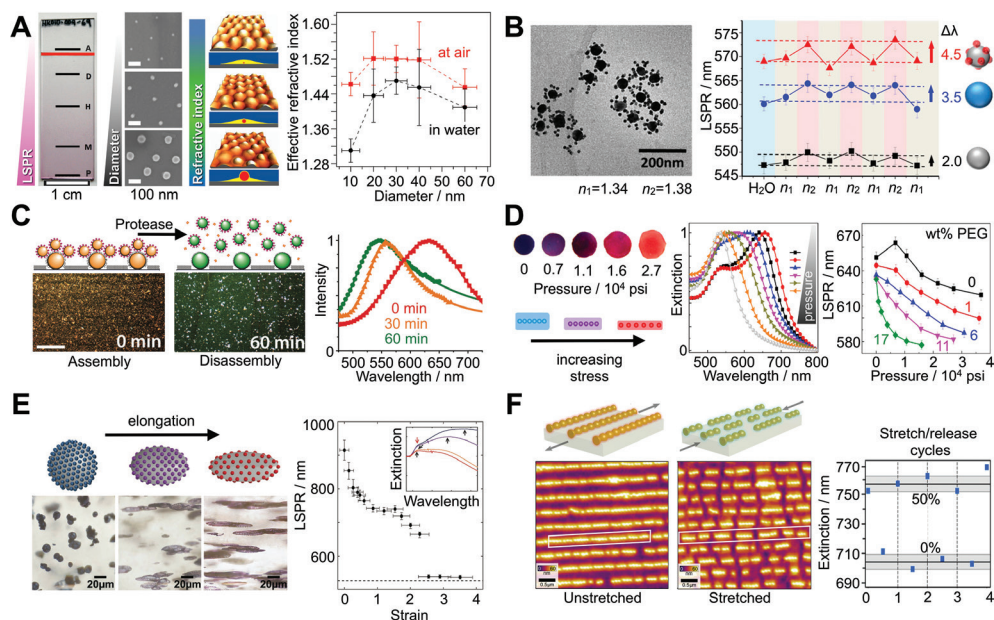
Figure 3. Colorimetric sensing concepts of ordered NP assemblies and defined patterned superstructures: (A) effective refractive index of a substrate-supported array of particles with a gradient in sizes. Copyright 2014 ACS, adapted with permission [51]. (B) Core/satellite assemblies for highly sensitive refractive index sensing. Copyright 2015 ACS, adapted with permission [52]. (C) Biomolecular detection by disassembly of core/satellite assemblies. Copyright 2011 ACS, adapted with permission [54]. (D) Stress memory sensor based on disassembly of AuNP chains. Copyright 2014 ACS, adapted with permission [56]. (E) Mechanochromic strain sensor based on AuNP-decorated microparticles dispersed in a polymer matrix. Copyright 2017 Wiley, adapted with permission [59]. (F) Reversible strain-induced fragmentation of quasi-infinite linear assemblies to defined plasmonic oligomers. Copyright 2017 ACS, adapted with permission [62].

satellite assemblies to optimize the spectral shift due to satellite attachment or release. They provided clear strategies for improving the sensitivity and signal-to-noise ratio for molecular detection, enabling simple colorimetric assays [53]. **Figure 3C** depicts the disassembly of substrate-supported core/satellite assemblies for biomolecular detection [54]. By addition of trypsin, the cysteine/biotin-streptavidin peptide tethers were proteolytically cleaved to release the satellites into solution enabling colorimetric detection of the protease.

Different concepts have been developed for opto-mechanic sensitivity and control [55]. Yin et al. reported a stress-responsive colorimetric film that can memorize the stress it has experienced (**Figure 3D**, left) [56]. This stress memory sensor is based on the LSPR shift associated with the disassembly of chains of AuNPs embedded in a polymer matrix (middle). By plastic deformation, the LSPR experiences a blueshift by irreversible breaking of the linear AuNP assemblies, initially formed in colloidal suspension [57]. The sensitivity of the optical change to stress could be tuned by doping with different amounts of PEG as plasticizer (right) [56]. Instead of mixing NPs with an elastic matrix, AuNPs can also be grown at the surface of a flexible substrate [58]. This enables mechanical control of the plasmonic coupling and electromagnetic fields at the surface. Dreyfus and coworkers designed mechanochromic AuNP-decorated microparticles as strain sensor (**Figure 3E**) [59]. After dispersion in an

elastic polymer matrix of PVA, the capsules change in color upon elongation. When the film is stretched, the capsules are deformed into elongated ellipsoidal shapes and the distance between the AuNPs, embedded in their shells, concomitantly increases. Another mechano-plasmonic approach has been proposed for substrate-supported chains of AuNPs. **Figure 3F** (left) shows oriented linear assemblies, above the so-called infinite chain limit [60, 61], in a periodic pattern over cm^2 areas on an elastic support [62]. Upon external strain, the assemblies experience a transition from long to short chains by reversible strain-induced fragmentation. The transition from plasmonic polymers to oligomers was accompanied by a pronounced spectral shift (right). A similar strain sensing approach was reported by Minati and coworkers using 1D arrays of broader line widths [63]. These multiparticle arrays showed a blueshift of the reflectance, lineally scaling with the external strain. Here, we will leave the field of colorimetric sensing and turn our attention to the enhancement of the electric field and the concomitant SERS activity.

3. SERS analytics

Since its discovery by Martin Fleischmann, Patrick J. Hendra, and A. James McQuillan in 1974, surface-enhanced Raman scattering has become an indispensable tool for analytical chemistry [64]. In this study, two types of pyridine adsorptions have been identified at Ag electrodes [65]. At the same time, the detected signal strengths were far beyond what could be expected to arise from local concentration of absorbed molecules. Later in 1977, two enhancement theories have been proposed independently, namely *chemical enhancement* [66] by Albrecht and Creighton and *electromagnetic enhancement* [67] by Jeanmaire and Van Duyne. Here, we will limit our discussion on the electromagnetic theory, because it is most closely linked to the optical and structural properties of nanocrystals and their assemblies. After an initial review of the origin of SERS enhancement [68, 69], we will go over prominent examples for the application of SERS for chemical spectroscopy.

3.1. From basic principles to off-resonance SERS enhancement

The Raman process describes the inelastic scattering of light by atoms or molecules discovered by C. V. Raman in 1928 [70]. This process has already been proposed theoretically by Adolf Smekal in 1923 [71]. In principle, Raman scattering builds on the interaction of a photon and a molecule (or crystal), for which an energy transfer can occur (**Figure 4A**) [72]. However, the Raman process has an inherently low cross-section because the probability of this transfer is *very low* and only 1 in 10^7 photons are scattered inelastically. For that reason, long measurement times are necessary to compensate for the low photon yield. Therefore, the low time resolution and the limitation of the spatial resolution demand on excellent optics. The SERS effect dramatically improves the photon yield, allowing to overcome these limitations. To clarify this, it is necessary to look at the origin of the enhancement [68].
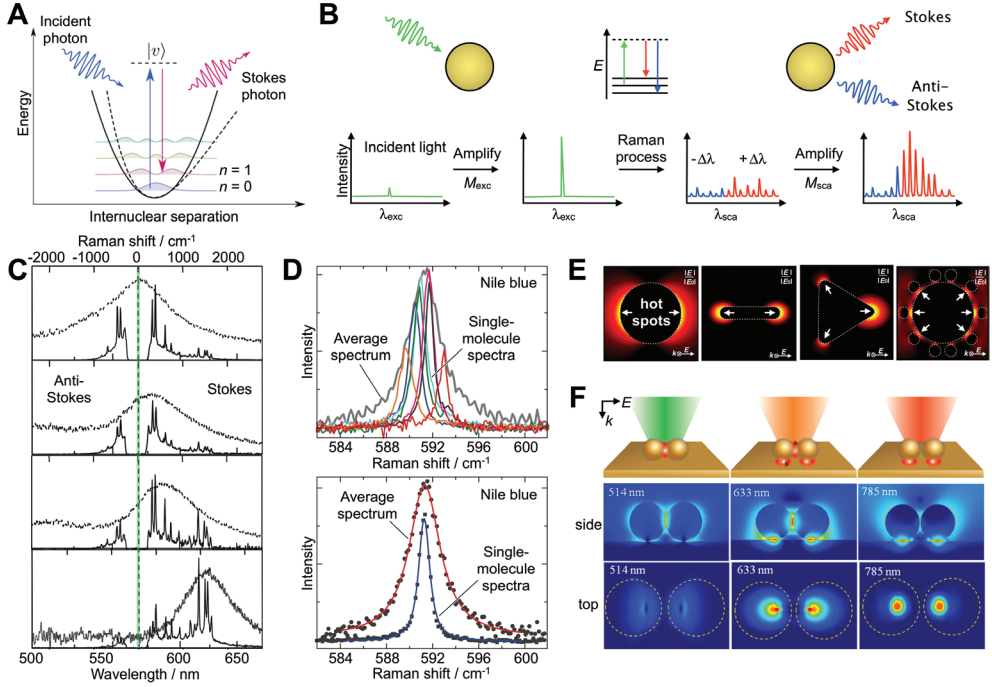
Figure 4. First principles of surface-enhanced Raman scattering: (A) schematic of the two-photon non-resonant stokes scattering between two vibrational states of a molecule ($n = 0$ -> $n = 1$) mediated by a virtual state v. A harmonic potential (solid line) approximates the energy landscape of the ground electronic level (dashed line). Copyright 2016 ACS, adapted with permission [72]. (B) Schematic of the twofold amplification process. (C) Single-molecule spectra of rhodamine Rh123 of AgNP aggregates (solid lines) reflecting the approximate shape of their corresponding Rayleigh scattering spectra (dotted lines). Copyright 2007 APS, adapted with permission [79]. (D) Comparison of individual single-molecule events to average signal (7500 spectra). Copyright 2010 ACS, adapted with permission [75]. (E) Electric field confinement of nanosphere, nanorod, nanotriangle, and core/satellite nanocluster; scaled to maximum visibility. Copyright 2016 ACS, adapted with permission [77]. (F) Selective excitation and spatial transfer of hot spots in dimer gap, in both junctions, or only in the particle–film junctions. Copyright 2016 ACS, adapted with permission [78].

3.1.1. The origin of the SERS enhancement

Raman scattering is, in its most basic and phenomenological form, the emission of a molecular Raman dipole ($\lambda_{sca} = \lambda_{exc} \pm \Delta\lambda$) [27]. Induced by the electric field E_{exc} of the exciting laser light λ_{exc}, a Raman dipole p_0 oscillates at a Raman-shifted frequency ($\omega_{sca} = 2\pi c/\lambda_{sca}$).

$$p_0(\omega_{sca}) = \alpha_0(\omega_{exc}, \omega_{sca})\ E_0(\omega_{exc}) \tag{3}$$

For a randomly oriented Raman scatterer, the radiated power is proportional to $|p_0|^2$ [68]. Thus, in order to enhance the Raman signal either the polarizability α or the electric field E need to be magnified. The first refers to chemical enhancement, this is the modification of the local

polarizability of the molecule (α_0 -> α_{loc}), whereas the latter is called electromagnetic enhancement EM and describes the augmentation and confinement of the local near-field (E_0 -> E_{loc}). The enhanced dipole p can be written as

$$p(\omega_{sca}) = \alpha_{loc}(\omega_{exc}, \omega_{sca})\ E_{loc}(\omega_{exc}) \tag{4}$$

Thus, the dipole enhancement upon excitation can be expressed by

$$\frac{|p|^2}{|p_0|^2} \propto \frac{|E_{loc}(\omega_{exc})|^2}{|E_0(\omega_{exc})|^2} = M_{exc}(\omega_{exc}) \tag{5}$$

Likewise, the dipole enhancement upon emission, that is, the Raman scatting, is given by

$$\frac{|p|^2}{|p_0|^2} \propto \frac{|E_{loc}(\omega_{sca})|^2}{|E_0(\omega_{sca})|^2} = M_{sca}(\omega_{sca}) \tag{6}$$

Although it is convenient from a theoretical point of view to separate the excitation and scattering into two steps, the Raman scattering process is instantaneous, and both occur simultaneously [27]. The combined enhancement M_{SERS} contains both contributions of the twofold amplification process (**Figure 4B**) [73]: the augmented excitation of a molecular dipole by an incident photon (λ_{exc}) and the stimulated emission of a scattered photon (λ_{sca}) of higher (anti-Stokes, $\lambda_{sca} < \lambda_{exc}$) or lower energy (Stokes, $\lambda_{sca} > \lambda_{exc}$).

$$M_{SERS}(\lambda_{exc}, \lambda_{sca}) = M_{exc}(\lambda_{exc}) \times M_{sca}(\lambda_{sca}) \tag{7}$$

Often, the total enhancement is simplified by the so-called $|E|^4$-approximation, which neglects the Raman shift. However, this approximation needs to be treated with caution as many cases have shown [74].

$$M_{exc}(\lambda_{exc}) \times M_{sca}(\lambda_{sca}) = \frac{|E_{loc}(\lambda_{exc})|^2}{|E_0(\lambda_{exc})|^2} \times \frac{|E_{sca}(\lambda_{sca})|^2}{|E_0(\lambda_{sca})|^2} \approx \frac{|E_{loc}(\lambda_{exc})|^4}{|E_0(\lambda_{exc})|^4} \tag{8}$$

The questions why and how the shapes of SERS spectra change has been addressed by Yamamoto and Itoh [73]. The transformation of the Raman spectrum, in principle the Raman cross section σ_{RS}, by the SERS process can be described as follows:

$$\sigma_{SERS} = M_{exc}(\lambda_{exc}) \times \sigma_{RS} \times M_{sca}(\lambda_{sca}) = \sigma_{RS} \times M_{SERS}(\lambda_{exc}, \lambda_{sca}) \tag{9}$$

If Eq. 9 holds true, this would enable the reconstruction of a SERS spectrum from the unenhanced Raman spectrum and an enhancement function $M_{SERS}(\lambda)$. Yamamoto and Itoh proposed that this reconstruction might be given by the product of the Raman spectrum times the Rayleigh scattering spectrum, based on observations using AgNP nanoaggregates (**Figure 4C**) [73]. They found that single-molecule spectra of rhodamine Rh123 (solid lines) were well reflecting the approximate shape of their corresponding Rayleigh scattering spectra (dotted lines) both for Stokes as well as Anti-Stokes scattering [43, 47]. **Figure 4D** shows a comparison of individual single-molecule events to average signal (7500 spectra) for Nile blue measured with Ag aggregates at high spectral resolution [75]. The ensemble averaging of many events revealed the characteristic broadening of the average spectrum (top) and fitted to Lorentzian line shapes (bottom).

All the reviewed examples, up to now, have capitalized from aggregated Ag nanocolloids as for example introduced by Lee and Meisel [76]. Such disordered aggregates enabled breakthrough results in regard to pushing the limit for ultrasensitive detection, down to single-molecule resolution, as well as nurtured the fundamental understanding of the origin of SERS enhancement. In the following section, we will turn our attention from disordered aggregated systems to individual nanocrystals and their ordered assemblies. The main aim is to find appropriate criteria for the design of nanostructures with both high and robust enhancement.

3.1.2. Hot spot formation

As a first step, we address the formation of *hot spots*, so-called confined locations of highest electric field strengths. For individual nanoparticles, hot spots can be found at the poles of nanospheres (e.g., in respect to an excited dipolar mode, see **Figure 4E**, left) or near areas of high surface curvatures, as at the tips of nanorods and nanotriangles (middle). In multiparticle systems, hot spots form inside interparticle gaps, cavities, or crevices, as depicted for an exemplary core/satellite assembly (right) [77]. Depending on the nature of the excited LSPR modes, and considering plasmonic hybridization in multiparticle systems, the distribution of hot spots can be quite diverse. For instance, the lighting of special hot spots has been demonstrated for film-coupled multiparticle configurations [78]. **Figure 4F** shows the basic example for selective excitation and spatial transfer of hot spots in a AuNP dimer. Depending on the excitation wavelength, the hot spots can be formed either in the dimer gap, in the particle-film junctions, or in both junctions at the same time [78]. Especially for complex systems, electromagnetic simulations can give valuable guidance for the design of targeted hot spots in plasmonic nanostructures [15, 23].

3.1.3. Off-resonance SERS enhancement

However, the design of NPs for SERS has shown to be more involved than simply maximizing the local electric field [80]. Murphy et al. initially reported the surprising finding of the highest SERS signals for LSPRs, blue-shifted from the wavelength of laser excitation. They studied an ensemble of Au nanorods of different aspect ratios (but uniform tip curvature) for which the longitudinal LSPRs shifted from 650 nm to 800 nm (**Figure 5A**, left). Contrary to expectations, the batches with matching of LSPR and laser excitation performed worse than off-resonant batches (right). This has been explained by a competition between SERS enhancement and extinction. The initial assumption that the LSPR is an adequate prediction for the best SERS performance has been shown to be incorrect.

Further validation was provided by a similar approach, screening the correlation of Au nanotriangle size and SERS performance [81]. Upon overgrowth, the LSPRs showed a continuous shift toward near-infrared (**Figure 5B**, left). Again, the highest SERS enhancement did not coincide with matching of the LSPR to the laser wavelength. Instead, the highest SERS activity was identified in off-resonance conditions (right). To rule out the influence of possible differences in tip/edge sharpness, the nanotriangle morphology was characterized by a close correlation of electron microscopy (TEM, field-emission SEM) and small-angle X-ray scattering (SAXS) analysis [50, 77, 81] combined with 3D atomistic modeling. This revealed a uniform tip curvature for all sizes.
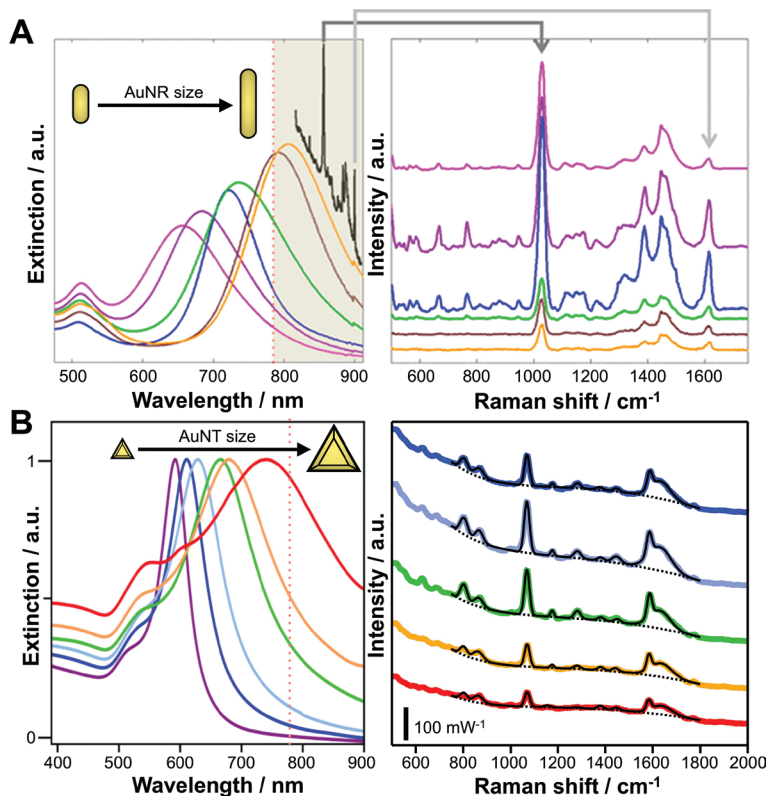
Figure 5. Off-resonance SERS enhancement: Non-linear dependency of (left) optical properties and (right) SERS signal intensities for variably sized (A) nanorods and (B) nanotriangles. (A) Copyright 2013 ACS, adapted with permission [80]. (B) Copyright 2018 ACS, adapted with permission [81].

The assumption that aggregation might be the cause for the off-resonant SERS activity was thoroughly investigated. Optical spectroscopy (UV-vis-NIR) before and after addition of the Raman marker did not show any indication of aggregation. Reversible aggregation/association of particles could be ruled out because of the presence of a sufficient amount of stabilizing agent (CTAB) in the solution. The amount of Raman marker (4MBA) added was much lower than that of the available stabilizing agent (>50-fold molar excess). The marker is not expected to act as a molecular linker. Also, in the case of irreversible aggregation, one would expect a loss of particles over time, which was not observed. The video feedback of the Raman microscopy did not give any indication of possible formation of aggregates even after the extended laser exposure. The colloidal dispersions were found to exhibit high colloidal stability for the reported surfactant concentrations, and the SERS signals could be detected reproducibly. Thus, even if aggregation (below the detection limit) was present, it would be of *negligible* contribution and should not have affected the registered SERS spectra [81].

Consequently, in many situations, the hot spot intensity *is not* directly correlated to the optical properties; thus, the extinction maximum is in many situations *not* the best excitation wavelength for SERS [81]. As a rule, an increase in SERS activity can be expected for situations in which the

Stokes-shifted Raman signals lies in the low-energy shoulder of the LSPR band; in other words, when the laser line is shifted to the red, compared to the LSPR extinction maximum.

3.2. SERS analytics of single particles

At this point, we move to the application of SERS for analytical purposes. The term "single or individual particles" indicates that the NPs are present in a dispersed state in colloidally stable dispersions and that aggregation is avoided. First, examples will be discussed that highlight the retrieval of chemical information at the NP surface. Then we will address the specific tasks of the different shells and its versatile functions for SERS applications.

3.2.1. Surface chemistry of nanoparticles in dispersion detection, exchange, competition, and chemical reaction of ligands

SERS analytics have proven to be a valuable tool for the detection, studies of the exchange and competitive adsorption, as well as localized chemical reactions of ligands at NP surfaces in dispersion.

Hafner et al. applied SERS analytics to study the structural transition in the surfactant layer that surrounds Au nanorods (**Figure 6A**, left) [82]. This was achieved by following the displacement of surfactant by thiolated poly(ethylene glycol). At the same time, they characterized the surfactant bilayer, revealing the absorbed layer of counterions at the gold surface Au^+X^-, the ammonium head group CN^+, as well as the skeletal vibrations of the alkane chain of the surfactant (right). Building on these findings, Chanana et al. investigated the quantitative exchange of surfactant against protein (bovine serum albumin) on Au nanorods (**Figure 6B**, left) [83]. In the context of biotoxicity, the cationic surfactant (CTA^+X^-) needs to be removed
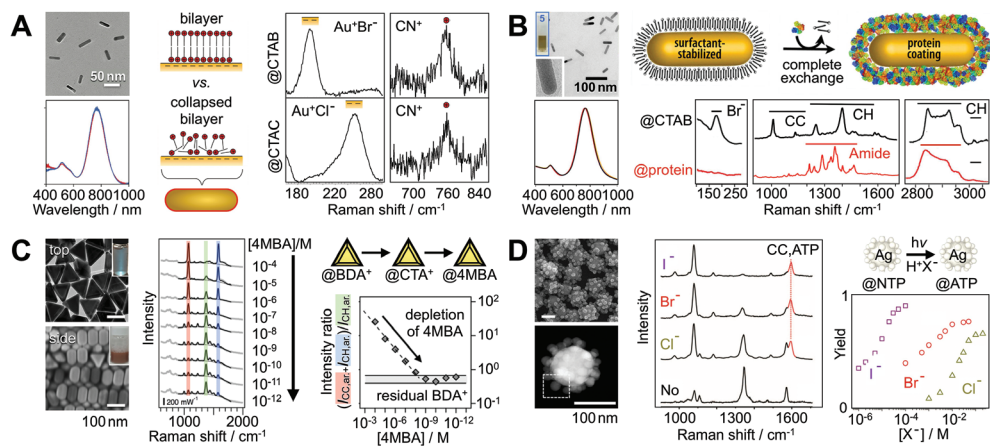

Figure 6. Detection, exchange, competition, and chemical reaction of ligands by SERS analytics in dispersion: (A) surfactant bilayer characterization on au nanorods (counter ion au$^+$X$^-$, ammonium head group CN$^+$). Copyright 2011 ACS, adapted with permission [82]. (B) Quantitative exchange of surfactant against protein on au nanorods. Copyright 2015 ACS, adapted with permission [83]. (C) Competition of aromatic surfactants (BDA$^+$), non-aromatic surfactants (CTA$^+$), and thiol ligands (4MBA) on au nanotriangles. Copyright 2018 ACS, adapted with permission [81]. (D) Hot electron-induced reduction of small ligands (NTP to ATP) on Ag core/satellite assemblies. Copyright 2015 NPG, adapted with permission [85].

from the solution and NP surface. This required to analyze the broad spectral range from 100 to 3100 cm^{-1}, covering all the characteristic signals associated with the ligand exchange (right). This evidenced the complete surfactant removal, which is a key step toward safe bioapplication of protein-coated NPs.

The competition of aromatic surfactants (BDA$^+$), non-aromatic surfactants (CTA$^+$), and thiol ligands (4MBA) was studied on Au nanotriangles (**Figure 6C**) [81]. Contrary to expectations, first evidence for the nonquantitative nature of the ligand exchange of aromatic versus non-aromatic surfactants was found. Differences in binding affinity toward the NP surface are attributed to additional π-interactions of the electron-rich benzyl headgroup [84]. It was possible to detect a trace amount of BDA$^+$ of 1–10 nM, which originated from the seed synthesis and could not be removed even after excessive washing with CTAB surfactant [81].

Schlücker and Xie applied SERS analytics to follow nano-localized chemistry on Ag core/satellite assemblies (**Figure 6D**, left) [85]. They reported the hot electron-induced reduction of small ligands (NTP to ATP) in the absence of chemical reduction agents. The reduction was found to depend on the available halide counterions X$^-$ (middle, right).

3.2.2. Functional shells for augmented SERS applications

The shell can provide for different functionalities, such as inertness, hosting of Raman markers, molecular trapping, harvesting/accumulation of analyte molecules, but also by means of improving the SERS activity.

The first examples represent chemically inert shells to protect SERS-active nanostructures from contact with whatever is being probed. This concept has been introduced by Tian et al. and entitled as shell-isolated NP-enhanced Raman spectroscopy (SHINERS) [86]. The silica shell acts as a nanoscale dielectric spacer. Such particles have been applied for the *in-situ* detection of pesticide contaminations on food/fruit [87]. Silica encapsulation can also be used to protect a molecular codification, a layer of Raman markers at the NP surface (**Figure 7A**) [88]. A silica shell enables further functionalization, chemical post-modification, and assembly of superstructures [89]. At the same time, silica overgrowth can stabilize superstructures as well as increase their colloidal stability and robustness (**Figure 7A**).

Pazos-Pérez and Alvarez-Puebla et al. demonstrated the SERS encoding of particles. For this, the NP surface is first partially functionalized by a stabilizing ligand, followed by a codification with a SERS marker (**Figure 7B**), and the final overcoating with silica to create an inert outer surface layer [90]. Also, hydrogel shells have shown to allow for molecular trapping of analyte molecules [91, 92]. The partial hydrophobic/hydrophilic nature of poly(N-isopropylacrylamide) during the reversible volume-phase transition can harvest analyte molecules from solution. After accumulation, the induced collapse of the shell can serve to increase the local concentration of analytes at the NP surface (**Figure 7C**, right) [93].

The shell can serve as a mean to improve the SERS activity of NPs. For example, as a template for the growth of complex NP morphologies. Liz-Marzán et al. developed an approach for the templated growth of branched Au structures inside of mesoporous silica shells (**Figure 7D**, left) [94]. The formed tips branching out from the cores (spheres, rods, triangles) improve the
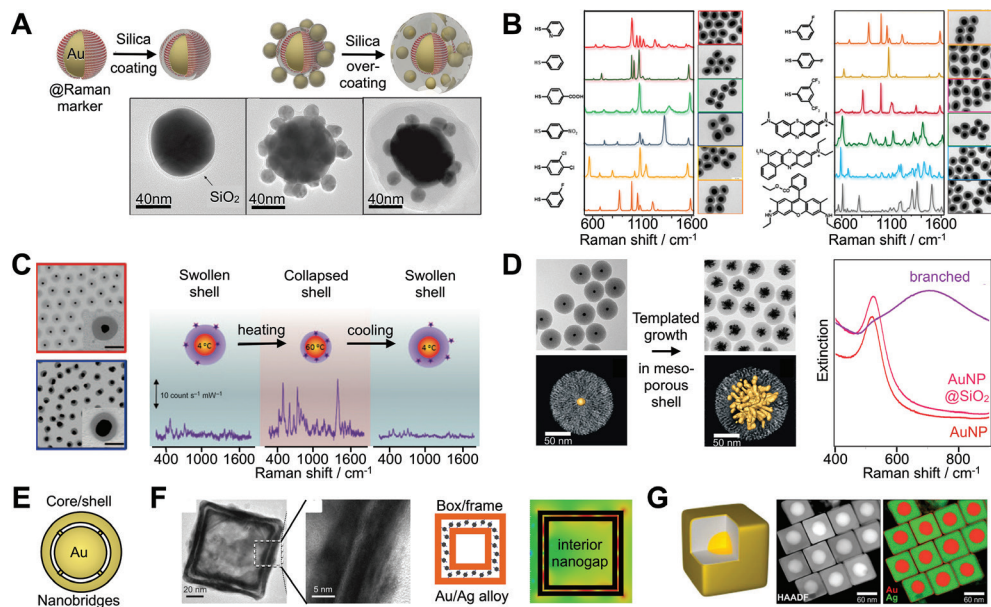
Figure 7. Functional shells for augmented SERS applications of single nanoparticles: (A) silica coating of dispersed AuNPs and overcoating of core/satellite superstructures. Copyright 2011 Wiley, adapted with permission [88]. (B) SERS-encoded NPs enclosed in silica. Copyright 2015 ACS, adapted with permission [90]. (C) Hydrogel-encapsulation for thermo-responsive molecular trapping. Copyright 2008 Wiley, adapted with permission [93]. (D) Branched morphologies grown inside radial mesoporous silica shells. Copyright 2015 ACS, adapted with permission [94]. (E) Schematic core/shell particle with nanoscale interior gaps and nanobridges [95]. (F) Interior nanogap within double-shelled au/Ag nanoboxes. Copyright 2015 NPG, adapted with permission [96]. (G) Protective au overcoating of AgNPs to increase their chemical stability. Copyright 2018 Wiley, adapted with permission [99].

plasmonic performance (right) while favoring the localization of analyte molecules at highly SERS-active regions. Another example is the formation of nanoscale DNA-tailorable interior gaps in spherical core/shell particles (**Figure 7F**) [95]. Interestingly, it has been found that the presence of nanobridges between shell and core does not perturb the hot spot formation. In **Figure 7G**, this concept is adopted for cubic NPs [96]. For such shelled Au/Ag nanoboxes and nanorattles, a pronounced electric field confinement was found in the interior nanocavity [50].

Metal overgrowth can increase surface roughness by forming bumpy structures [97] or undulated surfaces [98], which both showed increased SERS activity. At the same time, metal overgrowth can increase the chemical stability of NPs. A sub-skin depth Au layer has been shown to enable oxidant stability and functionality without altering the optical properties of Ag nanocubes (**Figure 7G**) [99].

3.3. SERS analytics of particle assemblies

The field of particle assemblies is sophisticated and versatile. Here, we start with disordered aggregates and then progressively move from small discrete oligomers to large organized multiparticle assemblies in dispersion or supported in substrates. The shown examples are

by no means to be considered universally valid but should serve as guidelines for a rational design of assemblies for SERS.

3.3.1. SERS sensing based on the formation of disordered aggregates under controlled conditions

In this section, we briefly delve back into the field of disordered aggregates to explore to what extent these can be formed under controlled conditions for SERS analytics. As introduced in Section 3.1, aggregates can exhibit high SERS activities but suffer from problems concerning reproducibility and robustness. Several approaches addressed these issues and proposed conditions under which aggregation can be induced in a controllable manner.

Gucciardi et al. reported the aggregation of Au nanorods mediated by optical forces and plasmonic heating (**Figure 8A**), for SERS detection of biomolecules at physiological pH [100]. The formed disordered NP clusters can embed molecules from solution, even in buffered media at neutral pH. The dynamics of the signal increase during aggregate formation have been studied revealing different states (**Figure 8B**: onset, stabilization, size increase, and saturation). The laser scattering and bright field images showed that such aggregates can reach micronscale dimensions after extended laser irradiation (over several tens of minutes). Aggregation can also be induced by specific binding, for example, glyco-conjugation of galectin-9 and glycan-decorated AuNPs. The real-time dynamic SERS sensing of galectin-9 in binding buffer, mimicking neutral conditions, revealed three different aggregation ranges, namely, an early, fast cluster growth, followed by a slower aggregation, before ultimately reaching the final equilibrium state [101]. Similarly, Mahajan et al. employed the selective guest sequestration of cucurbit[*n*]uril (CB[*n*]) molecules for molecular-recognition-based SERS assays (**Figure 8C**) [102]. These macrocyclic host molecules feature sub-nanometer dimensions capable of
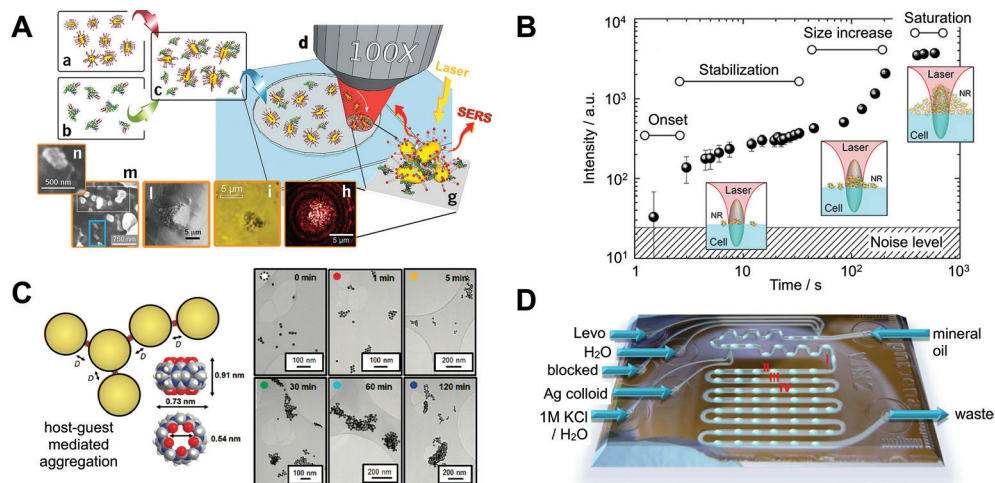

Figure 8. SERS sensing based on the formation of disordered aggregates under controlled conditions: (A) laser-induced aggregation by plasmonic heating and (B) aggregation dynamics. Copyright 2016 NPG, adapted with permission [100]. (C) Molecular-recognition-based SERS assay by selective guest sequestration. Copyright 2011 ACS, adapted with permission [102]. (D) Droplet-based microfluidic setup for lab-on-a-chip SERS measurements. Copyright 2016 ACS, adapted with permission [104].

binding AuNPs. The aggregation produces clusters with a defined interparticle spacing of 0.9 nm. The entitled "host-guest SERS" builds on the capturing of analyte guest molecules inside the barrel-shaped geometry of CB[*n*] host molecules [102, 103].

Lab-on-a-chip (LOC) SERS is an approach, particularly well-suited for diagnostic applications. **Figure 8D** depicts a droplet-based microfluidic setup for LOC SERS measurements [104]. For measurements, equal amounts of Ag colloids and buffer/analyte solutions were mixed and, finally, 1 M KCl was added for inducing the aggregation in a controlled and reproducible manner [105]. Such microfluidic devices with a liquid/liquid segmented flow, where analyte-containing droplets are formed in a carrier liquid like oil, show great potential for bioanalytics because minimal sample amounts are required and only short analysis times are needed, leading to significant cost reduction [106–108].

3.3.2. SERS sensing based on ordered assemblies designed for high SERS activity

The ultimate goal is to obtain full control over the organization of NPs into discrete clusters. In other words, finding appropriate conditions under which the local association of particles proceeds in a controlled way. This would give access to uniform and discrete assemblies of defined coordination numbers both in 2D and 3D.

The first step toward this goal was achieved by efficient fractionation of 3D clusters by density gradient separation. After purification, the mixed ensemble of clusters was separated yielding pure cluster populations (**Figure 9A**) [109]. The obtained fractions of monomers (single NPs), dimers, trimers, tetramers, pentamers, and higher species were characterized for their optical properties as well as their capabilities for SERS. The SERS activity per assembly was found to depend on the coordination number, which determines the number of available gaps in a cluster, but also the respective contribution of each gap.

For the case of substrate-supported "flat" clusters, Bach and coworkers fabricated core/satellite structures using DNA ligands to direct the self-assembly (**Figure 9B**) [110]. Such "nanoflower"-like 2D structures have shown improved SERS activity as compared to commercial SERS substrates. However, the critical parameter is the size ratio of core to satellite as it controls the coupling strength and plasmonic hybridization. For a high mismatch is sizes, this is for satellites of much smaller size than the core NP, the orbit of NPs is effectively uncoupled from the central NP. But the possible sensing applications of such structures go beyond the formation of hot spots for SERS. For matching building block sizes, Fano-like resonances have been predicted and experimentally observed for structures prepared by e-beam lithography [111–113]. Such resonances show the characteristic signature in the form of two LSPR peaks separated by a transparency window, a dip in extinction.

Building on this, one might ask what happens if such core/satellite patterns are formed on a curved surface, for example, a microparticle, or if the substrate consists of different metallic layers. The latter results in a complex architecture of multilayered core/satellite assemblies surrounding Au/Ag rattles as cores [114]. The rattles exhibit intrinsic hot spots inside the interior cavity between the central rod-like Au core and the frame of Au/Ag alloy [50, 115, 116]. By adsorption of small NPs at the exterior, the LSPR band broadened and shifted further toward red and additional extrinsic hot spots were formed. This broadening was found to be controlled by the density of the satellite particles.
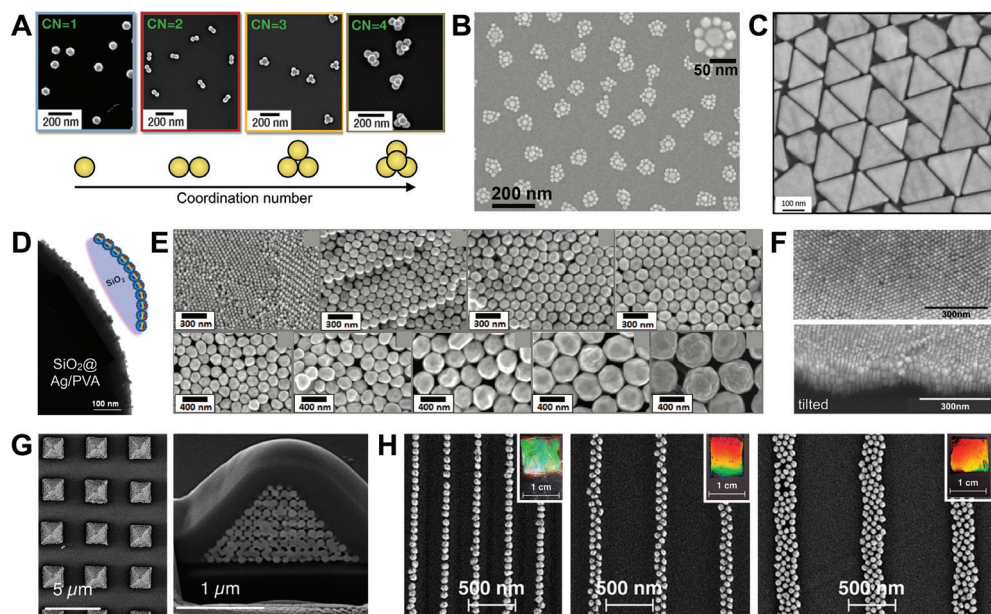
Figure 9. Ordered assemblies designed for high SERS activity. (A) Nanoparticle clusters of discrete coordination numbers. Copyright 2012 Wiley, adapted with permission [109]. (B) DNA-directed 2D core/satellite structures. Copyright 2012 Wiley, adapted with permission [110]. (C) Monolayer of close-packed nanotriangles. Copyright 2017 ACS, adapted with permission [118]. (D) AgNP-decorated silica microparticles. Copyright 2015 ACS, adapted with permission [119]. (E) Patterned supercrystal array of close-packed vertically aligned nanorods. Copyright 2012 Wiley, adapted with permission [124]. (F) Supercrystals of NPs ranging from the nano- to the microscale. Copyright 2012 ACS, adapted with permission [121]. (G) Pattern of pyramidal supercrystal architectures. Copyright 2017 ACS, adapted with permission [126]. (H) Macroscale patterns of quasi-infinite linear NP arrangements. Copyright 2014 ACS, adapted with permission [61].

In general, the density of assemblies is a critical parameter for SERS activity. The interparticle distances determine the coupling strength. Here, the coupling threshold of the smallest, in other words, the weakest coupling partner limits the interaction strength [117]. For a nanofilm, that is, a dense layer of close-packed particles, this limitation is overcome aided by collective long-range modes. For instance, a layer of nanotriangles prepared by film-casting and solvent evaporation shows nicely arranged edge-to-edge and tip-to-tip ordered arrangements in the monolayer (**Figure 9C**) [118]. The resulting extrinsic hot spots have been shown to allow for hot electron-driven catalytic reactions such as the dimerization of 4-NTP to 4,4'-dimercaptoazobenzene (DMAB), followed by SERS spectroscopy in a dry state. Radziuk and Möhwald reported close-packed nanofilms of 30-nm sized AgNPs on silica microparticles for intracellular SERS (**Figure 9D**) [119]. The primary (of individual microparticles) and secondary hot spots (between adjacent microparticles) were utilized for chemical imaging of live fibroblasts [120]. These AgNP-decorated microparticles have been compared to AgNPs with a 5 nm silica shell and silica NPs with a 5 nm thin Ag coating.

The nanofilm concept can be extended to thicker layers ultimately yielding supercrystals of close-packed NPs. **Figure 9F** presents a study in which supercrystals of NPs ranging from nano- to the microscale dimension have been realized [121]. During this transition, the LSPR band of the building blocks becomes increasingly broad because of higher polar modes. The formed superlattices exhibited pronounced interparticle coupling, whereas only the top layer is available for SERS sensing because of a limited penetration depth. However, also patterning can be utilized to discretize the electromagnetic response of the films/crystals. By comparison of different geometries of discrete supercrystals, it was found that patterning can have a deep impact on the surface electric field generation [122].

In addition to size, the shape of the used building block NPs plays an important role. For anisotropic particles such as nanorods, the local organization becomes essential. Organized nanorod supercrystals in lying-down [123] and standing configurations have shown significant contributions of side-to-side interactions between the close-packed NPs [124]. Bach et al. developed a method for directed nanorod assembly to prepare micropatterned substrates of vertically oriented nanorods (**Figure 9F**).

Finally, we turn our attention toward complex superstructures of organized NPs such as periodical arrays of pyramidal supercrystals. These superstructures accumulate the electric near-field at the apex of the pyramid [125]. The focalization can be expected to strongly depend on the "sharpness" of the pyramid but also on the internal order. Liz-Marzán and coworkers further developed the templated self-assembly to obtain "high quality" pyramids with highly ordered face-centered cubic lattices with one {100} facet oriented parallel to the pyramidal base and the {111} facets corresponding to the four lateral sides (**Figure 9G**) [126].

Further examples, highlighting the importance of structural order, are linear 1D assemblies with uniform interspaces. Here, lateral offsetting of NPs and inconsistent spacing can perturb the coupling along the chain [62, 127]. **Figure 9H** presents macroscale patterns of quasi-infinite linear NP arrangements [61]. The strong plasmonic coupling builds on the regular nanoscale spacing. Both, single-line and double-line arrays have been shown to provide for uniform enhancement, with higher values for the single-line arrays [128, 129]. Likewise, the use of anisotropic NPs, which is more challenging, causes the LSPRs to shift further toward the red [130].

Ultimately, the challenge in ordered systems is the control of the interparticle spacings because the gap sizes correlate with the achievable field enhancements. Here, the coating of the NPs plays an essential role, as it may act as a guide for the self-assembly but at the same time acts as a spacer in the final nanostructure [20].

4. Conclusion and outlook

This chapter gave an overview of plasmonics in the field of sensing. The state of the art offers a high diversity of accessible nanostructures. Starting with nanoparticles with specific morphological and optical properties up to the complex arrangements of these into ordered and even

hierarchical superstructures. Despite this diversity, it must be considered that the structure-property relations need to be well understood to design functional materials with tailored properties.

For colorimetric detection, this represents the fabrication of uniform systems with high spectral sensitivity. Both changes in particle size, shape, composition, and arrangement can be used for this purpose. This gave access to many possible applications in the field of biosensing, ion/temperature sensing, mechanosensing, among several others. In each case, the plasmonic response of a system to a specific internal or external stimulus represents the central design criterion. For colorimetry, the task of plasmonics is very direct, meaning that the plasmonic response of a material is evaluated directly. For this reason, the plasmonic material/substrate is often closely linked to the analytical question.

Building on this, SERS spectroscopy demonstrates the power of *surface-enhanced analytics*. Here, plasmonics serve to provide the enhancement as a means to an end. The central task is the detection of chemical information—often independent of the actual plasmonic material. In fact, the analysis is, in many cases, blind to the plasmonic material. This opens the door for optimizing the nanostructure for *higher signal yields*. In this overview, we have found various structural approaches to increase the sensitivity. The confined and localized enhancement in these structures gives access to unprecedented details about the chemistry of and at material interfaces and nanoparticle surfaces [131].

As a final thought, one needs to bear in mind that some open questions persist regarding the enhancement mechanism in action. For multiparticle systems and complex nanostructures, the prediction of hot spot localization and intensity becomes increasingly challenging. Several examples have shown the surprising circumstance of highest SERS response at unexpected conditions. In retrospect, it is likely that a fair share of SERS studies in the literature might be affected by particle aggregation. For that reason, targeted investigations are necessary to explain such phenomena. Also, the accurate prediction of SERS activity is still challenging both on a single-particle level as well as in multiparticle assemblies. In view of these points, besides increasing the sensitivity, the *sensing robustness* of the system must be a central design criterion in the development.

Acknowledgements

Conflict of interest

The author declares no competing financial interest.

Author details

Christian Kuttner[1,2,3]*

*Address all correspondence to: ckuttner@cicbiomagune.es

1 BioNanoPlasmonics Laboratory, CIC biomaGUNE, Donostia–San Sebastián, Spain

2 Leibniz-Institut für Polymerforschung Dresden e.V., Dresden, Germany

3 Cluster of Excellence Centre for Advancing Electronics Dresden (cfaed), Technische Universität Dresden, Dresden, Germany

References

[1] Howes PD, Chandrawati R, Stevens MM. Colloidal nanoparticles as advanced biological sensors. Science. 2014;**346**(6205):1247390

[2] Anker JN, Hall WP, Lyandres O, Shah NC, Zhao J, Van Duyne RP. Biosensing with plasmonic nanosensors. Nature Materials. 2008;**7**(6):442-453

[3] Bodelón G, Montes-García V, López-Puente V, Hill EH, Hamon C, Sanz-Ortiz MN, Rodal-Cedeira S, Costas C, Celiksoy S, Pérez-Juste I, Scarabelli L, La Porta A, Pérez-Juste J, Pastoriza-Santos I, Liz-Marzan LM. Detection and imaging of quorum sensing in Pseudomonas aeruginosa biofilm communities by surface-enhanced resonance Raman scattering. Nature Materials. 2016;**15**(11):1203-1211

[4] Zhang S, Geryak R, Geldmeier J, Kim S, Tsukruk VV. Synthesis, assembly, and applications of hybrid nanostructures for biosensing. Chemical Reviews. 2017;**117**(20):12942-13038

[5] Odom TW, Schatz GC. Introduction to plasmonics. Chemical Reviews. 2011;**111**(6): 3667-3668

[6] Faraday M. Experimental relations of gold (and other metals) to light. Philosophical Transactions. Royal Society of London. 1857;**147**:145-181

[7] Edwards PP, Thomas JM. Gold in a metallic divided state—from faraday to present-day nanoscience. Angewandte Chemie, International Edition. 2007;**46**(29):5480-5486

[8] Garnett JCM. Colours in metal glasses and in metallic films. Philosophical Transactions of the Royal Society A. 1904;**203**(359-371):385-420

[9] Mie G. Beitrage zur Optik trüber Medien, speziell kolloidaler Metallösungen. Annals of Physics. 1908;**330**(3):377-445

[10] Gans R. Über die Form ultramikroskopischer Goldteilchen. Annals of Physics. 1912; **342**(5):881-900

[11] Gans R. Über die Form ultramikroskopischer Silberteilchen. Annals of Physics. 1915; **352**(10):270-284

[12] Zsigmondy R, Norton JF, Spear EB. The chemistry of colloids. New York: John Wiley & Sons, Inc; 1917

[13] Myroshnychenko V, Rodríguez-Fernández J, Pastoriza-Santos I, Funston AM, Novo C, Mulvaney P, Liz-Marzan LM, Garcia de Abajo FJ. Modelling the optical response of gold nanoparticles. Chemical Society Reviews. 2008; **37**(9):1792-1805

[14] Zhang R, Bursi L, Cox JD, Cui Y, Krauter CM, Alabastri A, Manjavacas A, Calzolari A, Corni S, Molinari E, Carter EA, Garcia de Abajo FJ, Zhang H, Nordlander P. How to identify plasmons from the optical response of nanostructures. ACS Nano. 2017;**11**(7): 7321-7335

[15] Solís DM, Taboada JM, Obelleiro F, Liz-Marzan LM, Garcia de Abajo FJ. Toward ultimate nanoplasmonics modeling. ACS Nano. 2014;**8**(8):7559-7570

[16] Jiang N, Zhuo X, Wang J. Active plasmonics: Principles, structures, and applications. Chemical Reviews. 2018;**118**(6):3054-3099

[17] Liu K, Zhao N, Kumacheva E. Self-assembly of inorganic nanorods. Chemical Society Reviews. 2011;**40**(2):656-671

[18] Grzelczak M, Liz-Marzan LM. Colloidal nanoplasmonics: From building blocks to sensing devices. Langmuir. 2013;**29**(15):4652-4663

[19] Sharma B, Fernanda Cardinal M, Kleinman SL, Greeneltch NG, Frontiera RR, Blaber MG, Schatz GC, Van Duyne RP. High-performance SERS substrates: Advances and challenges. MRS Bulletin. 2013;**38**(8):615-624

[20] Kuttner C, Chanana M, Karg M, Fery A. Macromolecular decoration of nanoparticles for guiding self-assembly in 2D and 3D. In: Billon L, Borisov OV, editors. Macromolecular Self-Assembly. Hoboken, New Jersey: John Wiley & Sons, Inc; 2016:159-192 ISBN: 978-1118887127

[21] Kraus T, Brodoceanu D, Pazos-Perez N, Fery A. Colloidal surface assemblies: Nanotechnology meets bioinspiration. Advanced Functional Materials. 2013;**23**(36):4529-4541

[22] Hiltl S, Schuerings M-P, Balaceanu A, Mayorga V, Liedel C, Pich A, Boeker A. Guided self-assembly of microgels: From particle arrays to anisotropic nanostructures. Soft Matter. 2011;**7**(18):8231-8238

[23] Alvarez-Puebla R, Liz-Marzan LM, Garcia de Abajo FJ. Light concentration at the nanometer scale. Journal of Physical Chemistry Letters. 2010;**1**(16):2428-2434

[24] Halas NJ, Lal S, Chang W-S, Link S, Nordlander P. Plasmons in strongly coupled metallic nanostructures. Chemical Reviews. 2011;**111**(6):3913-3961

[25] Nordlander P, Oubre C, Prodan E, Li K, Stockman MI. Plasmon hybridization in nanoparticle dimers. Nano Letters. 2004;**4**(5):899-903

[26] Willets KA, Van Duyne RP. Localized surface plasmon resonance spectroscopy and sensing. Annual Review of Physical Chemistry. 2007;**58**(1):267-297

[27] Le Ru EC, Etchegoin PG. Quantifying SERS enhancements. MRS Bulletin. 2013;**38**(08): 631-640

[28] Schlücker S. Surface-enhanced Raman spectroscopy: Concepts and chemical applications. Angewandte Chemie, International Edition. 2014;**53**(19):4756-4795

[29] Cardinal MF, Vander Ende E, Hackler RA, McAnally MO, Stair PC, Schatz GC, Van Duyne RP. Expanding applications of SERS through versatile nanomaterials engineering. Chemical Society Reviews. 2017;**46**:3886-3903

[30] Barnes WL, Dereux A, Ebbesen TW. Surface plasmon subwavelength optics. Nature. 2003;**424**(6950):824-830

[31] Oates TWH, Wormeester H, Arwin H. Characterization of plasmonic effects in thin films and metamaterials using spectroscopic ellipsometry. Progress in Surface Science. 2011;**86**(11-12):328-376

[32] Guo X. Surface plasmon resonance based biosensor technique: a review. Journal of Biophotonics. 2012;**5**(7):483-501

[33] Yanase Y, Hiragun T, Ishii K, Kawaguchi T, Yanase T, Kawai M, Sakamoto K, Hide M. Surface plasmon resonance for cell-based clinical diagnosis. Sensors. 2014;**14**(3):4948-4959

[34] Roh S, Chung T, Lee B. Overview of the characteristics of micro- and nano-structured surface plasmon resonance sensors. Sensors. 2011;**11**(12):1565-1588

[35] Dhawan A, Canva M, Vo-Dinh T. Narrow groove plasmonic nano-gratings for surface plasmon resonance sensing. Optics Express. 2011;**19**(2):787-813

[36] Szunerits S, Boukherroub R. Sensing using localised surface plasmon resonance sensors. Chemical Communications. 2012;**48**(72):8999

[37] Chung T, Lee S-Y, Song EY, Chun H, Lee B. Plasmonic nanostructures for nano-scale bio-sensing. Sensors. 2011;**11**(12):10907-10929

[38] Miller MM, Lazarides AA. Sensitivity of metal nanoparticle surface plasmon resonance to the dielectric environment. The Journal of Physical Chemistry. B. 2005;**109**(46):21556-21565

[39] Jatschka J, Dathe A, Csáki A, Fritzsche W, Stranik O. Propagating and localized surface plasmon resonance sensing — a critical comparison based on measurements and theory. Sensing and Bio-Sensing Research. 2016;**7**:62-70

[40] Kreibig U. Hundert Jahre Mie-Theorie. Physik in Unserer Zeit. 2008;**39**(6):281

[41] Eustis S, El-Sayed MA. Why gold nanoparticles are more precious than pretty gold: noble metal surface plasmon resonance and its enhancement of the radiative and non-radiative properties of nanocrystals of different shapes. Chemical Society Reviews. 2006;**35**(3):209-217

[42] Atwater HA, Polman A. Plasmonics for improved photovoltaic devices. Nature Materials. 2010;**9**(3):205-213

[43] Yeh C-H, Zhao Z-Q, Shen P-L, Lin Y-C. Optimization of an optical inspection system based on the Taguchi method for quantitative analysis of point-of-care testing. Sensors. 2014;**14**(9):16148-16158

[44] McFarland AD, Van Duyne RP. Single silver nanoparticles as real-time optical sensors with zeptomole sensitivity. Nano Letters. 2003;**3**(8):1057-1062

[45] Rodríguez-Lorenzo L, la Rica de R, Alvarez-Puebla RA, Liz-Marzan LM, Stevens MM. Plasmonic nanosensors with inverse sensitivity by means of enzyme-guided crystal growth. Nature Materials. 2012;**11**(7):604-607

[46] Díez-Buitrago B, Briz N, Liz-Marzan LM, Pavlov V. Biosensing strategies based on enzymatic reactions and nanoparticles. Analyst. 2018;**143**(8):1727-1734

[47] Song JE, Cho EC. Dual-responsive and multi- functional plasmonic hydrogel valves and biomimetic architectures formed with hydrogel and gold nanocolloids. Scientific Reports. 2016;**6**:34622

[48] Laromaine A, Koh L, Murugesan M, Ulijn RV, Stevens MM. Protease-triggered dispersion of nanoparticle assemblies. Journal of the American Chemical Society. 2007;**129**(14): 4156-4157

[49] Pletsch H, Tebbe M, Dulle M, Förster B, Fery A, Förster S, Greiner A, Agarwal S. Reversible gold nanorod alignment in mechano-responsive elastomers. Polymer. 2015;**66**:167-172

[50] Schnepf MJ, Mayer M, Kuttner C, Tebbe M, Wolf D, Dulle M, Altantzis T, Formanek P, Förster S, Bals S, König TAF, Fery A. Nanorattles with tailored electric field enhancement. Nanoscale. 2017;**9**(27):9376-9385

[51] Müller MB, Kuttner C, König TAF, Tsukruk VV, Förster S, Karg M, Fery A. Plasmonic library based on substrate-supported gradiential plasmonic arrays. ACS Nano. 2014;**8**(9): 9410-9421

[52] Prasad J, Zins I, Branscheid R, Becker J, Koch AHR, Fytas G, Kolb U, Sönnichsen C. Plasmonic core–satellite assemblies as highly sensitive refractive index sensors. Journal of Physical Chemistry C. 2015;**119**(10):5577-5582

[53] Ross BM, Waldeisen JR, Wang T, Lee LP. Strategies for nanoplasmonic core-satellite biomolecular sensors: Theory-based design. Applied Physics Letters. 2009;**95**(19):193112

[54] Waldeisen JR, Wang T, Ross BM, Lee LP. Disassembly of a core–satellite nanoassembled substrate for colorimetric biomolecular detection. ACS Nano. 2011;**5**(7):5383-5389

[55] Maurer T, Marae-Djouda J, Cataldi U, Gontier A, Montay G, Madi Y, Panicaud B, Macias D, Adam P-M, Lévêque G, Bürgi T, Caputo R. The beginnings of plasmomechanics: towards plasmonic strain sensors. Frontiers of Materials Science. 2015;**9**(2):170-177

[56] Han X, Liu Y, Yin Y. Colorimetric stress memory sensor based on disassembly of gold nanoparticle chains. Nano Letters. 2014;**14**(5):2466-2470

[57] Liu Y, Han X, He L, Yin Y. Thermoresponsive assembly of charged gold nanoparticles and their reversible tuning of plasmon coupling. Angewandte Chemie, International Edition. 2012;**51**(26):6373-6377

[58] Cataldi U, Caputo R, Kurylyak Y, Klein G, Chekini M, Umeton C, Bürgi T. Growing gold nanoparticles on a flexible substrate to enable simple mechanical control of their plasmonic coupling. Journal of Materials Chemistry C. 2014;**2**:7927-7933

[59] Burel CAS, Alsayed A, Malassis L, Murray CB, Donnio B, Dreyfus R. Plasmonic-based mechanochromic microcapsules as strain sensors. Small. 2017;**13**(39):1701925

[60] Willingham B, Link S. Energy transport in metal nanoparticle chains via sub-radiant plasmon modes. Optics Express. 2011;**19**(7):6450-6461

[61] Hanske C, Tebbe M, Kuttner C, Bieber V, Tsukruk VV, Chanana M, König TAF, Fery A. Strongly coupled plasmonic modes on macroscopic areas via template-assisted colloidal self-assembly. Nano Letters. 2014;**14**:6863-6871

[62] Steiner AM, Mayer M, Seuss M, Nikolov S, Harris KD, Alexeev A, Kuttner C, König TAF, Fery A. Macroscopic strain-induced transition from quasi-infinite gold nanoparticle chains to defined plasmonic oligomers. ACS Nano. 2017;**11**(9):8871-8880

[63] Minati L, Chiappini A, Armellini C, Carpentiero A, Maniglio D, Vaccari A, Zur L, Lukowiak A, Ferrari M, Speranza G. Gold nanoparticles 1D array as mechanochromic strain sensor. Materials Chemistry and Physics. 2017;**192**:94-99

[64] Fleischmann M, Hendra PJ, McQuillan AJ. Raman spectra of pyridine adsorbed at a silver electrode. Chemical Physics Letters. 1974;**26**(2):163-166

[65] McQuillan AJ. The discovery of surface-enhanced Raman scattering. Notes and Records of the Royal Society of London. 2009;**63**(1):105-109

[66] Albrecht MG, Creighton JA. Anomalously intense Raman spectra of pyridine at a silver electrode. Journal of the American Chemical Society. 1977;**99**(15):5215-5217

[67] Jeanmaire DL, Van Duyne RP. Surface Raman spectroelectrochemistry. Journal of Electro analytical Chemistry and Interfacial Electrochemistry. 1977;**84**(1):1-20

[68] Etchegoin PG, Le Ru EC. Basic electromagnetic theory of SERS. In: Schlücker SS, editor. Surface enhanced Raman spectroscopy: Analytical, biophysical and life science applications. Weinheim: Wiley-VCH Verlag GmbH & Co. KGaA; 2011:1-37 ISBN: 978-3527325672

[69] Le Ru EC, Blackie E, Meyer M, Etchegoin PG. Surface enhanced Raman scattering enhancement factors: a comprehensive study. Journal of Physical Chemistry C. 2007;**111**(37):13794-13803

[70] Raman CV. A new radiation. Indian Journal of Physics. 1928;**2**:387-398

[71] Smekal A. Zur Quantentheorie der Dispersion. Naturwissenschaften. 1923;**11**(43):873-875

[72] Schmidt MK, Esteban R, González-Tudela A, Giedke G, Aizpurua J. Quantum mechanical description of Raman scattering from molecules in plasmonic cavities. ACS Nano. 2016;**10**(6):6291-6298

[73] Yamamoto YS, Itoh T. Why and how do the shapes of surface-enhanced Raman scattering spectra change? Recent progress from mechanistic studies. Journal of Raman Spectroscopy. 2016;**47**(1):78-88

[74] Graham D, Goodacre R, Arnolds H, Masson J-F, Schatz G, Baumberg J, Kim D-H, Aizpurua J, Lum W, Silvestri A, de Nijs B, Xu Y, Di Martino G, Natan M, Schlücker SS, Wuytens P, Bruzas I, Kuttner C, Hardy M, Chikkaraddy R, Sabanes NM, Delfino I, Dawson P, Gawinkowski S, Bontempi N, Mahajan S, Reich S, Hourahine B, Bell S, likowska AK, Porter M, Keeler A, Kamp M, Fountain A, Fasolato C, Giorgis F, Otero JC, Matricardi C, Van Duyne R, Lombardi J, Deckert V, Velleman L. Theory of SERS enhancement: general discussion. Faraday Discussions. 2017;**205**:173-211

[75] Etchegoin PG, Le Ru EC. Resolving single molecules in surface-enhanced Raman scattering within the inhomogeneous broadening of Raman peaks. Analytical Chemistry. 2010;**82**(7):2888-2892

[76] Lee PC, Meisel D. Adsorption and surface-enhanced Raman of dyes on silver and gold sols. The Journal of Physical Chemistry. 1982;**86**(17):3391-3395

[77] Höller RPM, Dulle M, Thomä S, Mayer M, Steiner AM, Förster S, Fery A, Kuttner C, Chanana M. Protein-assisted assembly of modular 3D plasmonic raspberry-like core/satellite nanoclusters: Correlation of structure and optical properties. ACS Nano. 2016;**10**(6):5740-5750

[78] Chen S, Meng L-Y, Shan H-Y, Li J-F, Qian L, Williams CT, Yang Z-L, Tian Z-Q. How to light special hot spots in multiparticle-film configurations. ACS Nano. 2016;**10**(1):581-587

[79] Itoh T, Yoshida K, Biju V, Kikkawa Y, Ishikawa M, Ozaki Y. Second enhancement in surface-enhanced resonance Raman scattering revealed by an analysis of anti-Stokes and Stokes Raman spectra. Physical Review B. 2007;**76**(8): DOI: 085405

[80] Sivapalan ST, Devetter BM, Yang TK, van Dijk T, Schulmerich MV, Carney PS, Bhargava R, Murphy CJ. Off-resonance surface-enhanced Raman spectroscopy from gold nanorod suspensions as a function of aspect ratio: Not what we thought. ACS Nano. 2013;**7**(3): 2099-2105

[81] Kuttner C, Mayer M, Dulle M, Moscoso A, López-Romero JM, Förster S, Fery A, Pérez-Juste J, Contreras-Cáceres R. Seeded growth synthesis of gold nanotriangles: Size control, SAXS analysis, and SERS performance. ACS Applied Materials & Interfaces. 2018;**10**(13):11152-11163

[82] Lee S, Anderson LJE, Payne CM, Hafner JH. Structural transition in the surfactant layer that surrounds gold nanorods as observed by analytical surface-enhanced Raman spectroscopy. Langmuir. 2011;**27**(24):14748-14756

[83] Tebbe M, Kuttner C, Männel M, Fery A, Chanana M. Colloidally stable and surfactant-free protein-coated gold nanorods in biological media. ACS Applied Materials & Interfaces. 2015;**7**(10):5984-5991

[84] Tebbe M, Kuttner C, Mayer M, Maennel M, Pazos-Perez N, König TAF, Fery A. Silver-overgrowth-induced changes in intrinsic optical properties of gold nanorods: From non invasive monitoring of growth kinetics to tailoring internal mirror charges. Journal of Physical Chemistry C. 2015;**119**(17):9513-9523

[85] Xie W, Schlücker S. Hot electron-induced reduction of small molecules on photorecycling metal surfaces. Nature Communications. 2015;**6**(1):467

[86] Tian X-D, Liu B-J, Li J-F, Yang Z-L, Ren B, Tian Z-Q. SHINERS and plasmonic properties of Au Core SiO_2 shell nanoparticles with optimal core size and shell thickness. Journal of Raman Spectroscopy. 2013;**44**(7):994-998

[87] Li J-F, Huang YF, Ding Y, Yang Z-L, Li S-B, Zhou XS, Fan FR, Zhang W, Zhou ZY, De Yin W, Ren B, Wang ZL, Tian Z-Q. Shell-isolated nanoparticle-enhanced Raman spectroscopy. Nature. 2010;**464**(7287):392-395

[88] Gellner M, Steinigeweg D, Ichilmann S, Salehi M, Schütz M, Kömpe K, Haase M, Schlücker S. 3D Self-assembled plasmonic superstructures of gold nanospheres: Synthesis and characterization at the single-particle level. Small. 2011;**7**(24):3445-3451

[89] Hanske C, Sanz-Ortiz MN, Liz-Marzan LM. Silica-coated plasmonic metal nanoparticles in action. Advanced Materials. 2018;**6**:1707003 DOI: 10.1002/adma.201707003

[90] Mir-Simon B, Reche-Perez I, Guerrini L, Pazos-Perez N, Alvarez-Puebla RA. Universal one-pot and scalable synthesis of SERS encoded nanoparticles. Chemistry of Materials. 2015;**27**(3):950-958

[91] Contreras-Cáceres R, Pastoriza-Santos I, Alvarez-Puebla RA, Pérez-Juste J, Fernández-Barbero A, Liz-Marzan LM. Growing Au/Ag nanoparticles within microgel colloids for improved surface-enhanced Raman scattering detection. Chemistry - A European Journal. 2010;**16**(31):9462-9467

[92] Casado-Rodriguez MA, Sanchez-Molina M, Lucena-Serrano A, Lucena-Serrano C, Rodriguez-Gonzalez B, Algarra M, Diaz A, Valpuesta M, Lopez-Romero JM, Pérez-Juste J, Contreras-Caceres R. Synthesis of vinyl-terminated Au nanoprisms and nanooctahedra mediated by 3-butenoic acid: Direct Au@pNIPAM fabrication with improved SERS capabilities. Nanoscale. 2016;**8**(8):4557-4564

[93] Alvarez-Puebla RA, Contreras-Cáceres R, Pastoriza-Santos I, Pérez-Juste J, Liz-Marzan LM. Au@pNIPAM colloids as molecular traps for surface-enhanced, spectroscopic, ultra-sensitive analysis. Angewandte Chemie, International Edition. 2008;**48**(1):138-143

[94] Sanz-Ortiz MN, Sentosun K, Bals S, Liz-Marzan LM. Templated growth of surface enhanced Raman scattering-active branched gold nanoparticles within radial mesoporous silica shells. ACS Nano. 2015;**9**(10):10489-10497

[95]   Lim D-K, Jeon K-S, Hwang J-H, Kim H, Kwon S, Suh YD, Nam J-M. Highly uniform and reproducible surface-enhanced Raman scattering from DNA-tailorable nanoparticles with 1-nm interior gap. Nature Nanotechnology. 2011;**6**(7):452-460

[96]   Zhang W, Rahmani M, Niu W, Ravaine S, Hong M, Lu X. Tuning interior nanogaps of double-shelled Au/Ag nanoboxes for surface-enhanced Raman scattering. Scientific Reports. 2015;**5**:8382

[97]   Shang Y, Shi J, Liu H, Liu X, Wang Z-G, Ding B. A bumpy gold nanostructure exhibiting DNA-engineered stimuli-responsive SERS signals. Nanoscale. 2018;**10**(20):9455-9459

[98]   Liebig F, Sarhan RM, Prietzel C, Thünemann AF, Bargheer M, Koetz J. Undulated gold nanoplatelet superstructures: in situ growth of hemispherical gold nanoparticles onto the surface of gold nanotriangles. Langmuir. 2018;**34**(15):4584-4594

[99]   Mayer M, Steiner AM, Röder F, Formanek P, König TAF, Fery A. Aqueous gold overgrowth of silver nanoparticles: merging the plasmonic properties of silver with the functionality of gold. Angewandte Chemie, International Edition. 2017;**56**(50):15866-15870

[100] Fazio B, D'Andrea C, Foti A, Messina E, Irrera A, Donato MG, Villari V, Micali N, Maragò OM, Gucciardi PG. SERS detection of biomolecules at physiological pH via aggregation of gold nanorods mediated by optical forces and plasmonic heating. Scientific Reports. 2016;**6**:26952

[101] Langer J, García I, Liz-Marzan LM. Real-time dynamic SERS detection of galectin using glycan-decorated gold nanoparticles. Faraday Discussions. 2017;**205**:363-375

[102] Taylor RW, Lee T-C, Scherman OA, Esteban R, Aizpurua J, Huang FM, Baumberg JJ, Mahajan S. Precise subnanometer plasmonic junctions for SERS within gold nanoparticle assemblies using cucurbit[n]uril "glue". ACS Nano. 2011;**5**(5):3878-3887

[103] Kim NH, Hwang W, Baek K, Rohman MR, Kim J, Kim HW, Mun J, Lee SY, Yun G, Murray J, Ha JW, Rho J, Moskovits M, Kim K. Smart SERS hot spots: single molecules can be positioned in a plasmonic nanojunction using host–guest chemistry. Journal of the American Chemical Society. 2018;**140**(13):4705-4711

[104] Hidi IJ, Jahn M, Pletz MW, Weber K, Cialla-May D, Popp J. Toward levofloxacin monitoring in human urine samples by employing the LoC-SERS technique. Journal of Physical Chemistry C. 2016;**120**(37):20613-20623

[105] Hidi IJ, Jahn M, Weber K, Cialla-May D, Popp J. Droplet based microfluidics: spectroscopic characterization of levofloxacin and its SERS detection. Physical Chemistry Chemical Physics. 2015;**17**(33):21236-21242

[106] Hidi IJ, Mühlig A, Jahn M, Liebold F, Cialla D, Weber K, Popp J. LOC-SERS: towards point-of-care diagnostic of methotrexate. Analytical Methods. 2014;**6**(12):3943

[107] Hidi IJ, Jahn M, Weber K, Bocklitz T, Pletz MW, Cialla-May D, Popp J. Lab-on-a-chip-surface enhanced Raman scattering combined with the standard addition method:

Toward the quantification of nitroxoline in spiked human urine samples. Analytical Chemistry. 2016;**88**(18):9173-9180

[108] Jahn IJ, Žukovskaja O, Zheng XS, Weber K, Bocklitz TW, Cialla-May D, Popp J. Surface-enhanced Raman spectroscopy and microfluidic platforms: Challenges, solutions and potential applications. Analyst. 2017;**142**(7):1022-1047

[109] Pazos-Perez N, Wagner CS, Romo-Herrera JM, Liz-Marzan LM, Garcia de Abajo FJ, Wittemann A, Fery A, Alvarez-Puebla RA. Organized plasmonic clusters with high coordination number and extraordinary enhancement in surface-enhanced Raman scattering (SERS). Angewandte Chemie, International Edition. 2012;**51**(51):12688-12693

[110] Zheng Y, Thai T, Reineck P, Qiu L, Guo Y, Bach U. DNA-directed self-assembly of core-satellite plasmonic nanostructures: A highly sensitive and reproducible near-IR SERS sensor. Advanced Functional Materials. 2012;**23**(12):1519-1526

[111] Dregely D, Hentschel M, Giessen H. Excitation and tuning of higher-order Fano resonances in plasmonic oligomer clusters. ACS Nano. 2011;**5**(10):8202-8211

[112] Yorulmaz M, Hoggard A, Zhao H, Wen F, Chang W-S, Halas NJ, Nordlander P, Link S. absorption spectroscopy of an individual Fano cluster. Nano Letters. 2016;**16**(10): 6497-6503

[113] Chang W-S, Lassiter JB, Swanglap P, Sobhani H, Khatua S, Nordlander P, Halas NJ, Link S. A plasmonic Fano switch. Nano Letters. 2012;**12**(9):4977-4982

[114] Xiong W, Sikdar D, Yap LW, Premaratne M, Li X, Cheng W. Multilayered core–satellite nanoassemblies with fine-tunable broadband plasmon resonances. Nanoscale. 2015;**7**(8):3445-3452

[115] Liu K-K, Tadepalli S, Tian L, Singamaneni S. Size-dependent surface enhanced Raman scattering activity of plasmonic nanorattles. Chemistry of Materials. 2015;**27**(15):5261-5270

[116] Jaiswal A, Tian L, Tadepalli S, Liu K-K, Fei M, Farrell ME, Pellegrino PM, Singamaneni S. Plasmonic nanorattles with intrinsic electromagnetic hot-spots for surface enhanced Raman scattering. Small. 2014;**267**(10):4287-4292

[117] Brown LV, Sobhani H, Lassiter JB, Nordlander P, Halas NJ. Heterodimers: Plasmonic properties of mismatched nanoparticle pairs. ACS Nano. 2010;**4**(2):819-832

[118] Liebig F, Sarhan RM, Sander M, Koopman W, Schuetz R, Bargheer M, Koetz J. Deposition of gold nanotriangles in large scale close-packed monolayers for X-ray-based temperature calibration and SERS monitoring of plasmon-driven catalytic reactions. ACS Applied Materials & Interfaces. 2017;**9**(23):20247-20253

[119] Radziuk D, Möhwald H. Surpassingly competitive electromagnetic field enhancement at the silica/silver interface for selective intracellular surface enhanced Raman scattering detection. ACS Nano. 2015;**9**(3):2820-2835

[120] Radziuk D, Schuetz R, Masic A, Moehwald H. Chemical imaging of live fibroblasts by SERS effective nanofilm. Physical Chemistry Chemical Physics. 2014;**16**:24621-24634

[121] Pazos-Perez N, Garcia de Abajo FJ, Fery A, Alvarez-Puebla RA. From nano to micro: Synthesis and optical properties of homogeneous spheroidal gold particles and their superlattices. Langmuir. 2012;**28**(24):8909-8914

[122] Tebbe M, Lentz S, Guerrini L, Fery A, Alvarez-Puebla RA, Pazos-Perez N. Fabrication and optical enhancing properties of discrete supercrystals. Nanoscale. 2016;**8**(25):12702-12709

[123] Tebbe M, Maennel M, Fery A, Pazos-Perez N, Alvarez-Puebla RA. Organized solid thin films of gold nanorods with different sizes for surface-enhanced Raman scattering applications. Journal of Physical Chemistry C. 2014;**118**(48):28095-28100

[124] Thai T, Zheng Y, Ng SH, Mudie S, Altissimo M, Bach U. Self-assembly of vertically aligned gold nanorod arrays on patterned substrates. Angewandte Chemie, International Edition. 2012;**51**(35):8732-8735

[125] Alba M, Pazos-Perez N, Vaz B, Formentin P, Tebbe M, Correa-Duarte MA, Granero P, Ferré-Borrull J, Alvarez R, Pallares J, Fery A, de Lera AR, Marsal LF, Alvarez-Puebla RA. Macroscale plasmonic substrates for highly sensitive surface-enhanced Raman scattering. Angewandte Chemie, International Edition. 2013;**52**(25):6459-6463

[126] Hanske C, González-Rubio G, Hamon C, Formentin P, Modin E, Chuvilin A, Guerrero-Martínez A, Marsal LF, Liz-Marzan LM. Large-scale plasmonic pyramidal supercrystals via templated self-assembly of monodisperse gold nanospheres. Journal of Physical Chemistry C. 2017;**121**(20):10899-10906

[127] Slaughter LS, Willingham BA, Chang W-S, Chester MH, Ogden N, Link S. Toward plasmonic polymers. Nano Letters. 2012;**12**(8):3967-3972

[128] Pazos-Perez N, Ni W, Schweikart A, Alvarez-Puebla RA, Fery A, Liz-Marzan LM. Highly uniform SERS substrates formed by wrinkle-confined drying of gold colloids. Chemical Science. 2010;**1**(2):174-178

[129] Mueller M, Tebbe M, Andreeva DV, Karg M, Alvarez-Puebla RA, Pazos-Perez N, Fery A. Large-area organization of pNIPAM-coated nanostars as SERS platforms for polycyclic aromatic hydrocarbons sensing in gas phase. Langmuir. 2012;**28**(24):9168-9173

[130] Tebbe M, Mayer M, Glatz BA, Hanske C, Probst PT, Mueller MB, Karg M, Chanana M, König TAF, Kuttner C, Fery A. Optically anisotropic substrates via wrinkle-assisted convective assembly of gold nanorods on macroscopic areas. Faraday Discussions. 2015;**181**:243-260

[131] Kuttner C. Macromolecular interphases and interfaces in composite materials. Dr. Hut Verlag München. 2014:1-359 ISBN: 978-3-8439-1845-9